

Contributions of climate change and groundwater extraction to soil moisture trends

Longhuan Wang^{1,2}, Zhenghui Xie^{1*}, Binghao Jia¹, Jinbo Xie¹, Yan Wang^{1,2}, Bin Liu^{1,2}, Ruichao Li^{1,2}, Si Chen^{1,2}

¹State Key Laboratory of Numerical Modeling for Atmospheric Sciences and Geophysical Fluid Dynamics, Institute of Atmospheric Physics, Chinese Academy of Sciences, Beijing 100029, China

²College of Earth Science, University of Chinese Academy of Sciences, Beijing 100049, China

Correspondence to: Zhenghui Xie (zxie@lasg.iap.ac.cn)

Abstract. Climate change affects water availability for soil, and groundwater extraction influences water redistribution by altering water demand, both of which significantly affect soil moisture. Quantifying their relative contribution to the changes in soil moisture will further our understanding of the mechanisms underlying the global water cycle. In this study, two groups of simulations were conducted with and without groundwater (GW) extraction (estimated based on local water supply and demand) from 1979–2010 using the land surface model CAS-LSM with four global meteorological forcing datasets (GSWP3, PRINCETON, CRU-NCEP, and WFDEI). To investigate the contribution of climate change and GW extraction, a trajectory-based method was used. Comparing the simulated results with the in-situ dataset of the International Soil Moisture Network (ISMN) and the satellite-based soil moisture product of the European Space Agency’s Climate Change Initiative (ESA-CCI) indicated that the CAS-LSM reasonably reproduced the distribution of soil moisture, and well matched the temporal changes. Globally, our results suggested a significant decreasing trend in surface soil moisture (0–10 cm, $0.98 \text{ e-}4 \text{ mm}^3 \text{ mm}^{-3} \text{ yr}^{-1}$) over the 32-year period tested. The drying trends were mainly observed in arid regions such as the tropical desert regions in North Africa and the Arabian Peninsula. While the wetting trends were primarily in tropical forested areas in South America and Northeast Asia. Climate change contributed 101.2% and 90.7% to global drying and wetting trends of surface soil moisture, respectively, while GW extraction accounted for -1.2% and 9.3% , respectively. In deep soil, GW extraction contributed 1.37% and -3.21% to the drying and wetting trends, respectively. The weak influence of GW extraction may be because this activity occurs in limited areas. GW extraction contributed more than 35%

29 to the change in surface soil moisture in wetting areas where GW overexploitation occurs. GW is mainly
30 extracted for irrigation to alleviate soil water stress in semiarid regions that receive limited precipitation,
31 thereby slowing the drying trend and accelerating the wetting trend of surface soil. However, GW
32 exploitation weakens the hydraulic connection between soil and aquifer, leading to deeper soils drying
33 up. Overall, climate change dominated the soil moisture trends, but the effect of GW extraction cannot
34 be ignored.

35 **1. Introduction**

36 Soil moisture plays a critical role in controlling the exchange of water, energy, and carbon between the
37 land–vegetation–water–atmosphere system (Seneviratne et al., 2010; van den Hurk et al., 2011). Soil
38 drying could increase the possibility of agricultural drought and fire (Dai et al., 2011), and affects plant
39 transpiration, photosynthesis, microbial activity, and a number of biogeochemical processes. Significant
40 decreasing trends in soil moisture can lead to water scarcity, threatening water supply and associated
41 food production (Döll et al., 2009; Wisser et al., 2010; Albergel et al., 2012; Wada et al., 2013; Dai, 2013;
42 Zhan et al., 2016). Soil moisture trends are affected by both climate (e.g., precipitation and temperature)
43 and human activities (e.g., groundwater (GW) extraction). Climate change can affect water availability
44 for soil (Dai, 2013; Wentz et al., 2007; Feng, 2016), and human activities influence the soil water content
45 through altering the surface water flux of soil (Min et al., 2011; Douville et al., 2013; Feng, 2016). GW
46 extraction, such as for irrigation, also has been shown to affect local soil moisture. However, it remains
47 unclear which of these factors exerts more influence owing to the complex interactions involved.
48 Therefore, quantifying the contribution of climate change and GW extraction to soil moisture trends will
49 improve our understanding of how human activities affect soil water content and will help to determine
50 the mechanisms underlying the global water cycle.

51 Traditionally, trends in soil moisture have been studied using ground-based observations (Robock et al.,
52 2005), which provide a direct record of soil moisture and are used as reference measurements for
53 calibrating other methods for measuring soil moisture (Yin et al., 2018). Since they are limited in space,
54 require significant manpower for sampling (Seneviratne et al., 2010), and cannot always represent larger

55 scales, remote sensing methods (e.g., passive and active microwave remote sensing) that provide global
56 coverage and excellent temporal sampling of soil moisture are widely used (Albergel et al., 2013).
57 Nevertheless, the accuracy of these measurements depends on the retrieval approach strongly, and
58 determining the contribution of climate and human activities is not easy. As a result, recent studies have
59 mostly relied on model estimates (Wei et al., 2008; Zhan et al., 2016).

60 **Land surface models (LSMs) can be used to calculate soil moisture trends at regional or global scales (Li**
61 **et al.,2011; Jia et al., 2018).** Different LSMs have been developed to simulate soil moisture as a function
62 of meteorological input variables and soil and vegetation parameters **over a few decades** (e.g., Kowalczyk
63 et al., 2006; Lawrence et al., 2011; Best et al., 2011). Much previous research has focused on the effect
64 of climate change on soil moisture using comprehensive LSMs forced with realistic forcing data (Berg
65 et al., 2003; Guo et al., 2006; Wei et al., 2008; Wang and Zeng, 2011). For the global average,
66 precipitation had a dominant effect on the variability of soil moisture at interannual to decadal time scales;
67 however, temperature was the main cause of the long-term trend in soil moisture. Increased soil drying
68 in the transitional regions was primarily caused by global warming, which is illustrated by regression
69 analysis and LSMs (Cheng and Huang, 2016). Since 1950, rising temperatures have contributed **45% to**
70 **the total soil moisture reduction (Cai et al., 2009).** In semiarid regions, precipitation and temperature are
71 equally important to the simulations of soil hydrological variables (Wang and Zeng, 2011). Jia et al.
72 (2018) found that precipitation controlled the direction of soil moisture changes **using remote sensing**
73 **data ESA-CCI and modeling of soil moisture by Community Land Model 4.5 (CLM4.5) in China.**

74 Recently, researchers have focused on incorporating human activity into the hydrological processes of
75 LSMs to assess the influence of anthropogenic activities on hydrological variable simulations. For
76 example, irrigation has been shown to affect soil water content through increased local
77 evapotranspiration and decreased temperatures near the surface (Yu et al., 2014; Zou et al., 2014). GW
78 over-extraction lowers GW tables, reduces total terrestrial water storage, weakens hydraulic connections
79 between aquifers and rivers, and may decrease lake area (Coe and Foley, 2001). Wada et al. (2013)
80 reported that human water consumption is one of the more important mechanisms intensifying
81 hydrological drought. GW exploitation caused drying in deep soil layers and wetting in upper layers,
82 lowering the water table and rapidly reducing terrestrial water storage with severe levels of GW
83 consumption (Zeng et al., 2016a, 2016b, 2017; Xie et al., 2018).

84 Thus, to our knowledge, the influence of anthropogenic activities (GW extraction) on soil moisture has
 85 not been explicitly quantified. Therefore, the main purpose of our study was to assess the relative
 86 contribution of GW extraction and climate change to soil moisture trends. To address this issue, the
 87 historical land simulations of the Land Surface, Snow and Soil moisture Model Intercomparison Project
 88 (LS3MIP) were employed (van den Hurk et al., 2016). Four global meteorological forcing datasets
 89 covering the 20th century were used with the land surface model for the Chinese Academy of Sciences
 90 (CAS-LSM), which considers human water regulation (HWR) and the movement of frost and thaw fronts
 91 (Xie et al., 2018). We compared the simulations with in-situ observations and the ESA CCI satellite-
 92 based product to validate the capacity of the CAS-LSM to simulate soil moisture trends. Furthermore,
 93 we investigated the interannual variation and trends in simulated soil moisture. Finally, the response of
 94 soil moisture temporal variability to climate change and GW extraction was investigated, which can
 95 further our understanding of the relationship between soil moisture and climate.

96 Section 2 describes the model used in this study, and describes the experimental designs, in-situ
 97 observations, and satellite-based data. Then Sect. 3 evaluates the soil moisture simulations in comparison
 98 with in-situ observations and satellite-based data. Also, the contributions of climate and GW extraction
 99 to soil moisture are discussed, while Sect. 4 outlines our conclusions.

100 **2. Model, data, and experimental design**

101 **2.1 Description of CAS-LSM**

102 Xie et al. (2018) incorporated GW lateral flow (GLF), Human Water Regulation (HWR), and the changes
 103 in the depth of frost and thaw fronts into CLM4.5 (Oleson, 2013) to develop the high-resolution CAS-
 104 LSM. For a detailed description of the physical processes within the CAS-LSM, see Xie et al. (2018). In
 105 the present study, only the HWR module was activated. Owing to the coarse resolution ($0.9^\circ \times 1.25^\circ$) of
 106 the experiment, it is not possible to describe the water intake of the river, that is, the surface water.
 107 Therefore, only GW extraction was considered in our study. Here, only the processes associated with
 108 soil water are briefly described below.

109 The following equation represents the total water balance of the hydrological system:

$$110 \Delta W_{can} + \Delta W_{sfc} + \Delta W_{sno} + \Delta W_{soil} + \Delta W_a = (q_{rain} + q_{sno} + q_s + q_g - ET_{veg,ground,hum} - q_{over} -$$

$$111 q_{h2osfc} - q_{drai} - q_{rgwl} - q_{ice}) \Delta t \quad \text{Eq. (1)}$$

112 where the left side denotes the change in canopy water, surface water, snow water, soil water, and ice
113 and water in the unconfined aquifer in turn. q_{rain} is rainfall, q_{sno} is snow, and q_s and q_g represent
114 the rate of surface and GW water use respectively, some of which will return to the soil. q_{over} is surface
115 runoff, q_{h2osfc} is runoff from surface water storage. q_{rgwl} and q_{ice} are liquid and solid runoff,
116 respectively, from glaciers, wetlands, and lakes. q_{drai} is subsurface drainage and $ET_{veg,ground,human}$
117 is evapotranspiration from vegetation, ground, and human water use. Δt is the time step(s).

118 2.2 Experimental setup

119 In this study, GSWP3 (Kim et al., 2016), WFDEI (Haddeland et al., 2011; Weedon et al., 2014), CRU-
120 NCEP (Viovy and Ciais, 2009), and PRINCETON (Sheffield et al., 2006) were used to run the offline
121 model. The fields included were air temperature, wind speed, specific humidity, solar radiation, and
122 precipitation. The GSWP3 is based on a dynamical downscaling of the 20th century reanalysis project
123 (Compo et al., 2011), covering the entire 20th century and some of the 21st century (1901–2012) at 0.5°
124 spatial resolution and 3-h intervals. The WATCH forcing data (WFD) are based on the ECMWF-ERA-
125 40 reanalysis data, and were also at 0.5° resolution and 3-h intervals, ceasing in 2001. A subsequent
126 project, EMBARCE, provided the WFDEI, which consisted of 3-h-interval ECMWF ERA-Interim
127 reanalysis data interpolated to 0.5° spatial resolution (1979–2014). Thus, there are offsets for some
128 variables in the overlap period with the WFD. The CRU-NCEP provided 6-h-interval data at 0.5°
129 horizontal spatial resolution (1901–2010). The PRINCETON is based on 6-h-interval surface climate
130 data from the NCEP-NCAR reanalysis. These data are available at 0.5° resolution and 3-h intervals. The
131 version used in this study is from 1901–2012 with a real-time extension based on satellite precipitation
132 and weather model analysis fields. General information about these datasets is summarized in Table 1.
133 Four forcing datasets were bilinearly interpolated to construct a field to a uniform 0.9° × 1.25° to ensure
134 that every simulation had the same soil and vegetation parameters.

135 We replaced the land cover data with the new generation of “land-use harmonization” (LUH2), which
136 builds on past work from CMIP5 (Hurtt et al., 2011). In addition, monthly irrigation datasets (Zeng et al.,
137 2016b) were used for land model runs, which were developed based on the Food and Agriculture
138 Organization of the United Nations (FAO) global water information system and the Global Map of
139 Irrigation Areas, version 5.0 (GMIA5; Siebert et al., 2005) and reflected the hydrological response to the
140 water consumption.

141 Two sets of numerical experiments were conducted using the default CLM4.5 (hereafter referred to as
142 CTL) and using the CAS-LSM with the HWR module activated (hereafter referred to as NEW). Thus,
143 CTL and NEW contained four simulations, CTL-GSWP3, CTL-CRUNCEP, CTL-PRINCETON, and
144 CTL-WFDEI (prefixed with NEW- for the NEW model). The CTL runs did not include GW extraction,
145 while the NEW runs did include it. Therefore, the difference between the NEW and CTL models would
146 provide a measure of the effect of GW extraction. Simulation spin up followed the TRENDY protocol
147 (<http://dgvm.ceh.ac.uk/node/9>) by recycling the climate mean and variability from 20 years (1901–1920)
148 of the meteorological forcing. Land use and CO₂ concentration were set to constant at the 1850 level
149 during spin up. All simulations were conducted with horizontal spacing of $0.9^\circ \times 1.25^\circ$. However, there
150 were differences among the four forcing datasets; therefore, the simulation period covers between 1901
151 and 2010 at a time step of 30 min. Considering that the ESA CCI was available from 1979–2010, our
152 evaluation focused on the same time interval.

153 **2.3 In-situ soil moisture and satellite-based data**

154 To evaluate the capability of the CAS-LSM to simulate soil moisture variation, we retrieved in-situ soil
155 moisture data from the International Soil Moisture Network (ISMN) (Robock et al., 2000; Dorigo et al.,
156 2011; Dorigo et al., 2013). The ISMN is based on in-situ measurements from different regional
157 monitoring projects. For our study, we used data from Africa, Asia, Europe, Australia, and North
158 America networks. Stations with >75% of the observational data missing during the evaluation period
159 were excluded. After which a subset of 225 stations remained (Fig. 3). There were only three dominant
160 contiguous areas in the world (the central USA, the North China Plain, and northern India) with severe
161 levels of GW extraction (Zeng et al., 2016b). Therefore, we focused on validating the ability of the model
162 to accurately represent the soil moisture in these three areas. Further site information is presented in
163 Table 2.

164 The European Space Agency's Climate Change Initiative (ESA CCI) involves remote sensing projects to
165 monitor global key climate variables with feedback effects on climate change. Soil moisture was then
166 included in 2010. There are three ESA CCI soil moisture products available based on the two types of
167 sensors employed by the project: active microwave remote sensing, passive microwave remote sensing,
168 and a combined product of both active and passive data. The active product was obtained using the SCAT
169 scatterometer and the METOP-A satellite-equipped C-band scatterometer using the algorithm proposed

170 by Wagner et al. (1999). The passive product includes observation data from four satellites, namely the
 171 tropical rainfall measuring mission microwave imager, the scanning multichannel microwave radiometer,
 172 the specific sensor microwave imager, and the advanced microwave scanning radiometer-Earth
 173 observing system. In the present study, we used the combined product (version 3.2), which covers 38
 174 years from 1978–2016 at a daily temporal resolution.

175 2.4 Analysis method

176 Taylor’s skill score (S) (Taylor, 2001) was used to quantitatively evaluate the spatial correlation of
 177 modeled soil moisture against the observations with standard deviations as follows:

$$178 \quad S = \frac{4(1+R)^4}{(\sigma_f + 1/\sigma_f)^2(1+R_0)^4} \quad \text{Eq. (2)}$$

179 where σ_f is the ratio of the standard deviation of the simulations to the observations, R is the spatial
 180 correlation coefficient between the simulation and observation, and R_0 is the maximum possible spatial
 181 correlation coefficient. As the model variance approaches the observed variance (i.e., as $\sigma_f \rightarrow 1$) and
 182 as $R \rightarrow R_0$, the skill approaches 1. Thus, a higher value of S indicates a better model performance, and
 183 $S = 1$ when the simulation and observation data are identical.

184 All simulated datasets were converted to annual means by averaging for the growing season (March–
 185 October) before the trend analysis. Precipitation and temperature were treated the same as soil moisture.
 186 Trends were calculated using the nonparametric Mann-Kendall test and the Theil-Sen median slope (Sen,
 187 1968) was used to delineate the trends.

188 To quantify the contribution of the climate and GW extraction to the trends in soil moisture, we used a
 189 trajectory method (Feng et al., 2014). **The “trajectory” refers to studying the change of GW extraction**
 190 **that occur within a certain period of time for a given grid or region. We can study the effect on soil**
 191 **moisture due to GW extraction in this way.** Soil moisture in the CTL experiment represented the effect
 192 of climate on soil moisture trends and served as a reference for isolating the contribution of GW
 193 extraction. The contributions were calculated with area weight summarization as follows:

$$194 \quad Con_{gw,global} = \frac{R_{gw}(T_{gw}-T_{ctl})}{T} \times 100\% \quad \text{Eq. (3)}$$

$$195 \quad Con_{cm,global} = (1 - Con_{gw,global}) \times 100\% \quad \text{Eq. (4)}$$

196 where $Con_{gw,global}$ and $Con_{cm,global}$ are the global contributions of GW extraction and climate,
 197 respectively; R_{gw} is the area ratio of GW extraction in the drying or wetting areas; T_{gw} and T_{ctl} are

198 the drying or wetting soil moisture trends in the GW and non-GW extraction regions, respectively; and
199 T is the soil moisture trend in the global drying or wetting zones.

200 Contributions of climate and GW extraction to certain grids were calculated as follows:

$$201 \quad Con_{gw,grid} = \frac{(T_{gw} - T_{ctl})}{T_{gw}} \times 100\% \quad \text{Eq. (5)}$$

$$202 \quad Con_{cm,grid} = (1 - Con_{gw,grid}) \times 100\% \quad \text{Eq. (6)}$$

203 where $Con_{gw,grid}$ and $Con_{cm,grid}$ are the contributions of GW extraction and climate to each grid,
204 respectively; T_{gw} and T_{ctl} are the soil moisture trends at each grid in the NEW and CTL experiments,
205 respectively.

206 **3. Results**

207 **3.1 Validation**

208 First, we compared the spatial distribution of simulated soil moisture with the ESA CCI product. Figure
209 1a, c, e, g shows the linear correlation coefficients between the ESA-CCI and the simulated top-10-cm
210 soil moisture time series from 1979-2010. The top-10-cm soil moisture is a weighted average of the first
211 four soil layer thicknesses (1.75, 2.76, 4.55, and 7.5 cm; the weights are 0.175, 0.276, 0.455, and 0.094,
212 respectively). The correlations between the simulated and ESA CCI data were significantly positive in
213 most areas ($r > 0.6$). Modeled results were more accurate in humid and temperature zones especially in
214 India and Southeast Asia ($r > 0.9$). Results revealed that the interannual variability of soil moisture cannot
215 be well captured in northern high-latitude areas (no correlation or negative correlations). This is partly
216 due to the limited ability of remote sensing technique in detecting soil moisture in frozen soils or under
217 snow cover.

218 Figure 1b, d, f, h shows the differences between NEW-simulations and ESA CCI data. Soil moisture
219 from all forcing datasets presented similar broad patterns. ESA-CCI had lower soil moisture compared
220 with the simulated results from Europe and the eastern USA. While Fig. 1f shows the results from CRU-
221 NCEP are drier than those from the other three at high latitudes in the northern hemisphere. The
222 simulation results in WFD were wetter overall, and the PRINCETON drier in South America and Central
223 Africa. However, overall, the results from PRINCETON and GSWP3 simulation were closer. Soil
224 moisture from NEW was 0.06% to 0.09% higher than that from CTL. The area represented by NEW is
225 irrigated; thus, the top 10 cm of soil is wetter in NEW than in CTL. However, the increase in soil moisture

226 was slight (about 0.001 to 0.2 mm³ mm⁻³). The differences between NEW and CTL indicate that **GW**
227 **extraction caused** a significant increase in top-10-cm soil moisture in the central USA, the North China
228 Plain, and North India. The three areas with severe levels of GW extraction (Fig. 2).
229 Figure 3 presents Taylor diagrams comparing the four NEW experiments with the in-situ ISMN
230 observations over the eight subregions (see Table 2 for site details). Figure 3 clearly shows that the model
231 can generally capture the changes in soil moisture in these regions (**with high correlation and close to 1**).
232 However, the performance of the model decreases as the soil depth increases. Results suggest that the
233 standard deviation ratios at most stations in Africa, Australia, Europe, and North America were **close to**
234 **1**, while those for India, Mongolia, China, and Former Soviet Union countries deviated from 1. Moreover,
235 the different forcing datasets did not perform similarly. GSWP performed relatively poorly in deep soil
236 in Europe, while PRINCETON provided a good estimation for Mongolia. CRUNCEP performed poorly
237 in China and Mongolia. In general, GSWP and WFDEI performed well, except for Europe and Mongolia.
238 Three areas (the central USA, North China Plain, and northern India) with severe levels of GW
239 exploitation were used as key areas for validation. The ground observations of soil moisture in the three
240 regions were retrieved from the ISMN. The usable stations were as follows: seven sites on the North
241 China Plain from 1981–1999, 15 sites in Colorado of central US from 2003–2010, and one site in Kanpur
242 of northern India from 2011–2012. The regional soil moisture from observations and simulations were
243 averaged from all stations and corresponding grid points. Before the comparison, hourly values from all
244 stations were converted into a monthly time series. The soil layer depths in the CAS-LSM did not match
245 those from the ground observations, and the depths of soil moisture observations varied among the three
246 regions. Therefore, we used different methods **to match the soil depth of observations to the**
247 **corresponding soil layer of simulations** for the different areas (Table 2).
248 We evaluated the performance of each forcing dataset over the three regions using Taylor’s skill scores,
249 as shown in Fig. 4 (left panel). As Fig. 4a shows, the individual forcing datasets show a varying ability
250 to capture the soil moisture distribution. In the 0–10 cm soil layer, WFD performed well and had the
251 highest skill scores ($S = 0.86$). Generally, all meteorological forcing datasets performed consistently well
252 for the North China Plain in both the near-surface and deeper soil layers. Performance was also evaluated
253 using a Taylor diagram as shown in Fig. 4d–f. GSWP captured the temporal variability of observed soil
254 moisture with higher correlations than the other datasets. Correlations tended to cluster around 0.7, with
255 the exception of CRUNCEP. Then, the correlations between observations and simulations decreased with

256 soil depth. The radial distance from the origin represents the standard deviation of simulations relative
257 to the standard deviation of observations. CRU-NCEP exhibited much higher ($\sigma_{\text{sim}}/\sigma_{\text{obs}} > 1$) variation than
258 that of the in-situ observations.

259 In the central US, WFD performed better with a higher skill score, and CRU-NCEP had the lowest score.
260 Correlations between the simulated 5-cm soil moisture and observations (Fig. 4e) were all lower than 0.5.
261 This may be because the offline runs do not consider the strong interaction between land and atmosphere.
262 All simulations resulted in lower standard deviations than those for observations at 50 cm soil depth.
263 This indicates that the true variability in soil moisture cannot be well reconstructed in this layer using the
264 four forcing datasets tested herein. Errors were also associated with the varying degrees of mismatch
265 between the soil layers of the observations and the model.

266 Owing to the limitations of the observational data in Kanpur, only three sets of data were compared in
267 that area. Based on the skill scores, WFD and PRINCETON performed well at both 10 cm and 25 cm
268 soil depths, and WFD performed better in deeper soil. The results of a correlation analysis indicated that
269 the simulations from three meteorological forcing datasets (GSWP3, PRINCETON, and WFD) were able
270 to capture the variation in soil moisture (Fig. 4f). Notably, the correlation was higher (>0.9 at North India)
271 when considering the GW extraction, which was not obvious in the other two areas (Fig. 4f). This is
272 because, according to FAO statistics, about 91% of GW extraction was to supply irrigation in India,
273 whereas 64% and 38% of GW extraction was used by agriculture in China and the USA, respectively
274 (Zeng et al., 2016b). Figure 4f shows that the relative standard deviations decreased as soil depth
275 increased, which indicates relatively large errors of fluctuation in the deeper soil layers. Overall, WFDEI
276 provided a better simulation with a higher correlation and a relative standard deviation close to 1.

277 **3.2 Trends in soil moisture**

278 Owing to the uncertainty in meteorological forcing, especially regarding precipitation, which had large
279 differences between different forcing datasets (Table 3), the ensemble average approach was used here.
280 Figure 5 presents the trends in surface soil moisture (0–10 cm), deep soil moisture (200–300 cm),
281 precipitation, temperature, and GW extraction from 1979–2010 from the NEW experiment. Globally,
282 results suggested a significant decreasing trend in surface and deep-soil moisture (-0.98 e-4 and -0.24
283 $\text{ e-4 mm}^3 \text{ mm}^{-3} \text{ yr}^{-1}$, respectively; $p < 0.05$) over the 32-year period, but the soil moisture trend from
284 PRINCETON was not significant (Table 3). There was a consistent significant warming trend (about

285 0.016°C yr⁻¹; $p < 0.05$) and a non-significant decreasing precipitation trend ($p > 0.05$). Furthermore, the
286 drying of the surface soil moisture slowed when considering the HWR. The global surface soil moisture
287 decreased at a rate of $-0.99 \text{ e-}4 \text{ mm}^3 \text{ mm}^{-3} \text{ yr}^{-1}$ without GW extraction. Conversely, the deep soil dried
288 ($-0.21 \text{ e-}4 \text{ mm}^3 \text{ mm}^{-3} \text{ yr}^{-1}$ in CTL) owing to the rapid lowering of the water table following GW
289 extraction, and the hydraulic connection between the soil and aquifer weakened. More specifically, GW
290 extraction slowed the drying of surface soils in drying areas and increased the wetting trend in wetting
291 areas. The trend in 1.3% of GW extraction areas changed from drying to wetting, with an average GW
292 extraction rate of 171 mm yr⁻¹. The opposite effect was observed in the deeper soil layers.

293 Figure 6 shows the spatial distribution of soil moisture trends from 1979–2010 obtained from simulations
294 of surface- and deep-soil moisture and ESA CCI. As the depth of the soil increased, the proportion of
295 apparent dryness increased. For the surface soil, the drying trends were mainly found in North Africa,
296 Central Asia, Southwestern USA, Southeast Australia. The wetting trends were primarily in northern
297 South America, northwest Africa, and northeast Asia. This result is consistent with those of previous
298 studies on satellite-based data (Feng, 2015; Dorigo et al., 2012). The trend in the deep soil was consistent
299 with that in the surface layer in most areas, except for Central Asia. Regions with a drying trend always
300 coincided with statistically significant increasing temperature. Many of the strong drying trends occurred
301 over regions that already have relatively low soil moisture. Drying trends were the most prominent in the
302 Sahel in northern Africa. This could be explained by deficits in precipitation during the 1970s and 1980s
303 (Hulme, 1992; L'Hôte et al., 2002). The majority of north Asia exhibited wetting trends with non-
304 significant increasing temperature. Wetting trends were found in the central US, India, and North China
305 Plain, but there were no significant changes.

306 We further evaluated the ratios of drying/wetting trends for surface and deep soil in different climate
307 regions using the Köppen-Geiger climate classification (Kottek et al., 2006). A brief description of the
308 climate classification is as follows: the first letter refers to the climate types: tropical (A), arid (B),
309 temperate (C), and cold (D). The second letter indicates the precipitation conditions: rainforest (f),
310 monsoon (m), and savannah (s) in tropical and desert (W) and steppe (S) in arid, dry summer (s), dry
311 winter (w), and without dry season (f) in temperate and cold climates. The third letter refers to hot (h)
312 and cold (k) in arid and hot summer (a), warm summer (b), cold summer (c), and very cold summer (d)
313 in temperate and cold climates. At the same time, we used the climate regions defined by Feng et al.
314 (2015), the first climate letter labelled Arid was the arid regions, the second letter “f” was the humid

315 regions and the other regions were the transitional regions. As Figure 7a shows, some arid regions became
316 significantly drier (16.9%) or wetter (9.8%); as did some humid regions (9.8% drier, 9.5% wetter) and
317 transitional regions (12.8% drier, 5.4% wetter). The area of increasing wetness in the Af subregion, which
318 is characterized by tropical rainforests, comprised 22% of its total area. The Dfd subregion is
319 characterized by areas without a dry season and 42.6% of this region rapidly became wetter (about 1.2
320 $e-3 \text{ mm}^3 \text{ mm}^{-3} \text{ yr}^{-1}$). Conversely, 21.5% of the BWh subregion, which is characterized by hot deserts,
321 was drying. In the Ds and Dw subregions, which have a hot summer or winter in a year, 30–40% was
322 drying out with a moisture decreasing rate more than $-1.2 e-3 \text{ mm}^3 \text{ mm}^{-3} \text{ yr}^{-1}$. These results indicate
323 that the drying trends were mainly in arid regions, while the wetting trends were primarily in humid
324 regions. Figure 7b shows that there are proportionally more significant changes in the deeper soil layers.
325 However, the changes are not as great as those in the surface soil. In arid regions (BW and BS subregions),
326 the proportion of apparent drying exceeded 40%. In humid regions (Cfc, Dfc, and Dfd subregions), 30–
327 71% of these areas were significantly wetting. The climatic zone differences in deep soil changes were
328 basically consistent with those in the topsoil, except in Dwc and Dwd regions.

329 **3.3 Contribution of climate change and GW extraction to soil moisture trends**

330 The trend in soil moisture was basically consistent with climate change, but the role of GW extraction
331 was **not** negligible. Then we quantified the relative contribution of climate and GW intake to the soil
332 moisture trends using the trajectory approach [Eqs. (2)–(3)]. Results showed that -1.2% of the significant
333 drying trends in the surface soil originated from GW extraction. Thus, the contribution of climate was
334 101.2% . Regarding the wetting trends, the contribution was 9.3% for GW extraction, with climate
335 contributing 90.7% . In deep soil, GW extraction contributed 1.37% and -3.21% to the drying and wetting
336 trends, respectively. This indicates that GW extraction only weakly contributes to global wetting and
337 drying trends. This is mainly due to the limited regions of GW extraction. The contribution of GW
338 extraction to surface soil moisture trends is presented in Fig. 8a. In the drying regions, GW extraction
339 and climate change accounted for -19.91% and 119.91% , respectively. **Notably, the negative**
340 **contribution is because that the surface soil moisture is decreasing, while GW extraction slows down the**
341 **reduction trend (but still decreasing), $T_{gw} - T_{cti}$ in Eqs. (5) is positive, but T_{gw} is negative.** In the
342 wetting regions, the contributions were 11.55% and 88.45% , respectively. GW exploitation is mainly
343 used for irrigation to increase moisture in the surface soil, which slows the drying of the surface soil,

344 promoting wetting. Figure 8b shows the contribution of GW extraction in the deeper soil layers. GW
345 extraction positively contributed to the drying trends (109.7%) and negatively contributed to the wetting
346 trends (-5.48%). This indirectly reflects that GW exploitation weakens the hydraulic connection between
347 soil and aquifers. In summary, GW is exploited to provide irrigation, which alleviates water stress in the
348 surface soil, and the deep soil dries due to the loss of hydraulic connection.

349 As shown in Fig. 8, the contribution of GW extraction mainly occurs in northern Africa, the North China
350 Plain, and central US. Thus, the three regions were selected for further evaluation. Figure 9 further shows
351 the relative contributions to soil moisture trends in three subregions. Contributions of GW extraction to
352 surface soil moisture wetting and drying trends were evident on the North China Plain (drying, up to
353 -62.39%; wetting, 77.74%), northern India (drying, up to -13.56%; wetting, 72.1%), and central US
354 (drying, -57.42%; wetting, 38.51%). For deep soil, the contribution of GW extraction was: North China
355 Plain (drying, 15.12%; wetting, -18.16%), northern India (drying, 56.54%; wetting, 2.07%), and central
356 USA (drying, 23.8%; wetting, -20%). GW extraction can increase the water content of the surface soil,
357 and thus leads to increased moisture in both humid and arid regions. The results revealed that GW
358 extraction contributes more to the soil moisture trends in typical exploitation areas than in the regions
359 without GW extraction. Climate change dominated the soil moisture trends, while the contribution of
360 GW extraction at the regional scale was much greater than that at the global scale, especially in the areas
361 with GW overexploitation.

362 **4. Conclusions and discussion**

363 In the present study, we quantified the relative contribution of climate and GW extraction to soil moisture
364 trends using a LSM (CAS-LSM) that considers HWR based on four global meteorological forcing
365 datasets. Comparing the simulations, the in-situ observational datasets, and the satellite-based ESA-CCI
366 surface products demonstrated that the CAS-LSM is able to reliably represent soil moisture trends.

367 The main conclusions of this study are as follows. First, all four forcing data resulted in similar patterns
368 of surface soil moisture, and have higher soil moisture than ESA-CCI. Results at the regional scale (Fig.
369 4) indicated that the uncertainty of the forcing data affected the simulated soil moisture. Therefore, the
370 ensemble average results were used to reduce the uncertainty caused by the forcing data. Second, our
371 results show a significant decreasing trend in surface and deep soil moisture over the 32-year period

372 investigated. For the surface soil, GW extraction slowed the drying trend in drying areas and increased
373 the wetting trend in wetting areas. This is because GW extraction is mainly used for irrigation as effective
374 water input into the topsoil. While has opposite effect on deep soil when the hydrological connection
375 between the aquifer and deep soil was weakened due to the extraction severely. Third, climate contributed
376 101.2% and 90.7% to global drying and wetting trends of surface soil moisture, while GW extraction had
377 a relative weak effect on soil moisture (-1.2% and 9.3% for global drying and wetting, respectively). For
378 deep soil, GW extraction contributed 1.37% and -3.21% to the drying and wetting trends. This is because
379 there are limited areas that exploit GW. Regionally, GW extraction contributed more in regions with high
380 water demand for irrigation, production, and human consumption. In typical water-use areas, including
381 the North China Plain, Central US, and North India, GW extraction contributed more to the soil moisture
382 trends than in the regions almost without GW extraction. In summary, climate change dominates the soil
383 moisture trends, while GW extraction accelerates or decelerates soil moisture trends under climate
384 change.

385 Our study demonstrated the effect of GW extraction on soil moisture. Future research should focus on
386 developing strategies to adapt to climate change. At the same time, the effect of GW exploitation on
387 regional soil moisture cannot be ignored. Over-exploitation weakens the hydraulic connection between
388 soil and aquifer, which may affect root growth and development. **Furthermore, GW extraction also
389 impact atmosphere. Zeng et al. (2016b) found that the cooling caused by GW extraction in northern India
390 weakened the Indian monsoon and its water vapor transport and the precipitation decreased. Therefore,
391 the development and utilization of water resources must consider the local ecological and atmospheric
392 environment.**

393 The mismatch of soil layers between the simulations and observations may affect the evaluation results.
394 Also, our results indicate that it is necessary to consider human activities in LSMs, and improved
395 descriptions of hydrological processes in LSMs are required. For example, GW extraction is assumed to
396 be occur in the area it is consumed in. Moreover, meteorological forcing data can introduce uncertainty
397 for simulation results. The precipitation data used in our study showed significant differences. The WFD
398 precipitation evidently decreased (1.96 mm yr^{-1}), and the GSWP precipitation slightly decreased (0.16
399 mm yr^{-1}), while for CRU-NCEP and PRINCETON, precipitation slightly increased. Temperature varied
400 similarly for all four forcing datasets (slightly increasing). The ensemble averaging method used in this
401 study is not the optimum choice. However, considering that the purpose of this study was to explore the

402 contribution of GW extraction to soil moisture trends, this simple averaging approach was reasonable. It
403 is necessary to use a more appropriate averaging method to minimize the uncertainty caused by the
404 forcing data in future work.

405 Future studies should focus on two aspects. First, GW extraction should be improved to reflect realistic
406 levels of water consumption. The GW extraction scheme used in this study is a simple bottom-up
407 representation, the irrigation demand is the water required to bring the soil moisture to saturation at each
408 time step, which describes an extreme water requirement and significantly overestimates the actual
409 irrigation water demand. Next work will focus on a more realistic definition of irrigation water demand,
410 such as the demand based on the difference between the potential evapotranspiration and available water.
411 Thus, simulations using the improved model would more accurately reflect hydrological effects and
412 enhance water resource management. Second, since only the effect of HWR was discussed in this study,
413 other human activities could also be considered. For instance, the association between soil moisture and
414 land-cover change can be evaluated. Changes in land-surface cover affect the hydrothermal properties of
415 the surface soil, which further affects soil moisture.

416 **Acknowledgements.** This work was jointly supported by the National Natural Science Foundation of
417 China (Grants 41830967), the National Key R&D Program of China (2018YFC1506602) and by the Key
418 Research Program of Frontier Sciences, CAS (QYZDY-SSW-DQC012). The ESA CCI soil moisture
419 dataset was downloaded from <http://www.esa-soilmoisture-cci.org>; the in-situ soil moisture observations
420 were downloaded from http://www.geo.tuwien.ac.at/insitu/data_viewer/ISMN.php.

421 **References**

422 Albergel, C., Rüdiger, C., Pellarin, T., Calvet, J. C., Fritz, N., Froissard, F., Suquia, D., Petitpa, A.,
423 Piguet, B., and Martin, E.: From near-surface to root-zone soil moisture using an exponential filter:
424 An assessment of the method based on in-situ observations and model simulations. *Hydrology and*
425 *Earth System Sciences*, 12(6), 1323–1337, 2008.

426 Albergel, C., de Rosnay, P., Gruhier, C., Muñoz-Sabater, J., Hasenauer, S., Isaksen, L., Kerr, Y., and
427 Wagner, W.: Evaluation of remotely sensed and modelled soil moisture products using global
428 ground-based in-situ observations, *Remote Sens. Environ.*, 118, 215–226, 2012.

429 Albergel, C., Dorigo, W., Balsamo, G., Muñoz-Sabater, J., De Rosnay, P., and Isaksen, L., Brocca, L.,
430 de Jeu, R., and Wagner, W.: Monitoring multi-decadal satellite earth observation of soil moisture
431 products through land surface reanalyses, *Remote Sens. Environ.*, 138, 77-89, 2013.

432 Berg, Aaron A.: Impact of bias correction to reanalysis products on simulations of North American soil
433 moisture and hydrological fluxes, *Journal of Geophysical Research*, 108(D16):ACL 2-1-ACL 2-
434 15, 2003.

435 Best, M. J., Pryor, M., Clark, D. B., Rooney, G. G., Essery, R. L. H., Ménard, C. B., Edwards, J. M.,
436 Hendry, M. A., Porson, A., Gedney, N., Mercado, L. M., Sitch, S., Blyth, E., Boucher, O., Cox, P.
437 M., Grimmond, C. S. B., and Harding, R.J.: The Joint UK Land Environment Simulator (JULES),
438 model description– Part 1: energy and water fluxes, *Geosci. Model Dev*, 4, 677–699, 2011.

439 Cai, W., Cowan, T., Briggs, P., and Raupach, M.: Rising temperature depletes soil moisture and
440 exacerbates severe drought conditions across southeast Australia, *Geophysical Research Letters*,
441 36(21), 272-277, 2009.

442 Calvet, J. C., Fritz, N., Froissard, F., Suquia, D., Petitpa, A., and Pignatelli, B.: In-situ soil moisture
443 observations for the CAL/VAL of SMOS: The SMOSMANIA network, *Proceedings of the IEEE
444 International Geoscience and Remote Sensing Symposium (IGARSS)*, 2008.

445 Cappelaere, B., Descroix, L., Lebel, T., Boulain, N., Ramier, D., Laurent, J.-P., Favreau, G., Boubkraoui,
446 S., Boucher, M., Moussa, I. B., Chaffard, V., Hiernaux, P., Issoufou, H. B. A., Le Breton, E.,
447 Mamadou, I., Nazoumou, Y., Oï, M., Otlé, C. and Quantin, G.: The AMMA-CATCH experiment

448 in the cultivated Sahelian area of south-west Niger - Investigating water cycle response to a
449 fluctuating climate and changing environment, *Journal of Hydrology*, 375(1-2), 34–51, 2009.

450 Cheng, S. J., and Huang, J. P.: Enhanced soil moisture drying in transitional regions under a warming
451 climate, *Journal of Geophysical Research: Atmospheres*, 121(6):2542-2555, 2016.

452 Coe, M. T., and Foley, J. A.: Human and natural impacts on the water resources of the lake chad basin,
453 *Journal of Geophysical Research: Atmospheres*, 106(D4), 3349-3356, 2001.

454 Compo, G. P., Whitaker, J. S., Sardeshmukh, P. D., Matsui, N., Allan, R. J., Yin, X., Gleason, B. E.,
455 Vose, R. S., Rutledge, G., Bessemoulin, P., Brönnimann, S., Brunet, M., Crouthamel, R. I., Grant,
456 A. N., Groisman, P. Y., Jones, P. D., Kruk, M. C., Kruger, A. C., Marshall, G. J., Maugeri, M.,
457 Mok, H. Y., Nordli, Ø., Ross, T. F., Trigo, R. M., Wang, X. L., Woodruff, S. D., and Worley, S.
458 J.: The Twentieth Century Reanalysis Project, *Quart. J. Roy. Meteor. Soc.*, 137, 1–28, 2011.

459 Dai, A. G.: Characteristics and trends in various forms of the palmer drought severity index during
460 1900–2008, *Journal of Geophysical Research: Atmospheres*, 116(D12), 2011.

461 Dai, A. G.: Increasing drought under global warming in observations and models, *Nature Climate*
462 *Change*, 3(1), 52-58, 2013.

463 de Rosnay, P. D., Gruhier, C., Timouk, F., Baup, F., Mougin, E., and Hiernaux, P., Kergoat, L., and
464 LeDantec, V.: Multi-scale soil moisture measurements at the Gourma meso-scale site in mali.
465 *Journal of Hydrology (Amsterdam)*, 375(1-2), 241-252, 2009.

466 Dorigo, W.A., Wagner, W., Hohensinn, R., Hahn, S., Paulik, C., Xaver, A., Gruber, A., Drusch, M.,
467 Mecklenburg, S., van Oevelen, P., Robock, A., and Jackson, T.: The International Soil Moisture
468 Network: A data hosting facility for global in-situ soil moisture measurements, *Hydrology and*
469 *Earth System Sciences*, 15 (5), 1675-1698, 2011.

470 Dorigo, W.A., Jeu, R.D., Chung, D., Parinussa, R., Liu, Y., Wagner, W., and Fernández-Prieto, D.:
471 Evaluating global trends (1988–2010) in harmonized multi-satellite surface soil moisture,
472 Geophysical Research Letters, 39(18), 18405, 2012.

473 Dorigo, W. A. , Xaver, A. , Vreugdenhil, M. , Gruber, A. , Hegyiová, A., Sanchis-Dufau, A. D., Zamojski,
474 D., Cordes, C., Wagner, W., and Drush, M.: Global automated quality control of in-situ soil
475 moisture data from the international soil moisture network, Vadose Zone Journal, 12(3), 918-924,
476 2013.

477 Döll, P., Fiedler, K. and Zhang, J.: Global-scale analysis of river flow alterations due to water
478 withdrawals and reservoirs, Hydrol. Earth Syst. Sci. 13 2413–32, 2009.

479 Douville, H., Ribes, A., Decharme, B., Alkama, R. and Sheffield, J. Anthropogenic influence on
480 multidecadal changes in reconstructed global evapotranspiration, Nature Clim. Change 3, 59–62,
481 2013.

482 Feng, H. H., and Liu, Y. B.: Trajectory based detection of forest-change impacts on surface soil moisture
483 at a basin scale [Poyang Lake Basin, China], J. Hydrol. 514, 337–346, 2014.

484 Feng, H. H., and Zhang, M. Y.: Global land moisture trends: drier in dry and wetter in wet over land,
485 Sci. Rep. 5, 18018; doi: 10.1038/srep18018, 2015.

486 Feng, H. H.: Individual contributions of climate and vegetation change to soil moisture trends across
487 multiple spatial scales, Sci. Rep. 6, 32782; doi: 10.1038/srep32782, 2016.

488 Guo, Z., Dirmeyer, P., Zeng, Z. H., Gao, X., and Zhao, M.: Evaluation of the Second Global Soil
489 Wetness Project soil moisture simulations: 2. Sensitivity to external meteorological forcing, J.
490 Geophys. Res., 111, D22S03, <https://doi.org/10.1029/2006JD007845>, 2006.

491 Haddeland, I., Clark, D. B., Franssen, W., Ludwig, F., Voß, F., Arnell, N. W., Bertrand, N., Best, M.,
492 Folwell, S., Gerten, D., Gomes, S., Gosling, S. N., Hagemann, S., Hanasaki, N., Harding, R.,
493 Heinke, J., Kabat, P., Koirala, S., Oki, T., Polcher, J., Stacke, T., Viterbo, P., Weedon, G. P., and
494 Yeh, P.: Multimodel Estimate of the Global Terrestrial Water Balance: Setup and First Results,
495 *Journal of Hydrometeorology.*, 12, 869–884, 2011.

496 Hulme, M.: Rainfall changes in africa: 1931–1960 to 1961–1990, *International Journal of Climatology*,
497 12(7), 685-699, 1992.

498 Hurr, G. C., Chini, L. P., Froking, S., Betts, R. A., Feddema, J., Fischer, G., Fisk, J. P., Hibbard, K.,
499 Houghton, R. A., Janetos, A., Jones, C. D., Kindermann, G., Kinoshita, T., Goldewijk, K. K., Riahi,
500 K., Shevliakova, E., Smith, S., Stehfest, E., Thomson, A., Thornton, P., van Vuuren, D. P., and
501 Wang, Y. P.: Harmonization of land-use scenarios for the period 1500–2100: 600 years of global
502 gridded annual land-use transitions, wood harvest, and resulting secondary lands, *Climatic Change*,
503 109(1-2), 117, 2011.

504 Jia, B. H., Liu, J. G., Xie Z. H., and Shi, C. X.: Interannual variations and trends in remotely sensed and
505 modeled soil moisture in China, *Journal of Hydrometeorology.* 19, 831-847, 2018.

506 Kim, H., Watanabe, S., Chang, E.-C., Yoshimura, K., Compo, G. P., Hirabayashi, Y., Famiglietti, J.,
507 and Oki, T.: A century-long global surface meteorology for offline terrestrial simulations, in
508 preparation, 2016.

509 Kowalczyk, E.A., Wang, Y.P., Law, R.M., Davies, H.L., McGregor, J.L., and Abramowitz, G.: The
510 CSIRO Atmosphere Biosphere Land Exchange (CABLE) model for use in climate models and as
511 an offline model. CSIRO Marine and Atmospheric Research Paper 013:
512 http://www.cmar.csiro.au/e-print/open/kowalczyka_2006a.pdf, 2006.

513 Kottek, M., Grieser, J., Beck, C., Rudolf, B. and Rubel, F.: World Map of the Köppen-Geiger climate
514 classification updated, Meteorol. Z15, 259–263, 2006.

515 Lawrence, D. M., Oleson, K. W., Flanner, M. G., Thornton, P. E., Swenson, S. C., Lawrence, P. J., Zeng,
516 X. B., Yand, Z. L., and Levis, S.: Parameterization improvements and functional and structural
517 advances in version 4 of the Community Land Model, Journal of Advances in Modeling Earth
518 Systems, 3, M03001, 2011.

519 L' Hôte Y, Mahé G, Somé B, and Triboulet JP.: Analysis of a sahelian annual rainfall index from 1896
520 to 2000; the drought continues, International Association of Scientific Hydrology Bulletin, 47(4),
521 10, 2002.

522 Li, M., Ma, Z. G., and Niu, G. Y.: Modeling spatial and temporal variations in soil moisture in China.
523 Chin. Sci. Bull., 56, 1809–1820, <https://doi.org/10.1007/s11434-011-4493-0>, 2011.

524 Marczewski, W., Slominski, J., Slominska, E., Usowicz, B., Usowicz, J., Romanov, S., Maryskevych,
525 O., Nastula, J., and Zawadzki, J.: Strategies for validating and directions for employing SMOS
526 data, in the Cal-Val project SWEX (3275) for wetlands. Hydrology and Earth System Sciences
527 Discussions, 7, 7007–7057, 2010.

528 Min, S-K., Zhang, X. B., Zwiers, F. W. and Hegerl, G. C.: Human contribution to more-intense
529 precipitation extremes, Nature 470, 378–382, 2011.

530 Mougin, E., Hiernaux, P., Kergoat, L., Grippa, M., de Rosnay, P., Timouk, F., Le Dantec, V., Demarez,
531 V., Lavenu, F., Arjounin, M., Lebel, T., Soumaguel, N., Ceschia, E., Mougenot, B., Baup, F.,
532 Frappart, F., Frison, P. L., Gardelle, J., Gruhier, C., Jarlan, L., Mangiarotti, S., Sanou, B., Tracol,
533 Y., Guichard, F., Trichon, V., Diarra, L., Soumaré, A., Koité, M., Dembélé, F., Lloyd, C., Hanan,
534 N. P., Damesin, C., Delon, C., Serca, D., Galy-Lacaux, C., Seghieri, J., Becerra, S., Dia, H.,

535 Gangneron, F., and Mazzega, P.: The AMMA-CATCH Gourma observatory site in Mali: Relating
536 climatic variations to changes in vegetation, surface hydrology, fluxes and natural resources.
537 *Journal of Hydrology*, 375, 14–33, 2009.

538 Oleson, K: Technical description of version 4.5 of the Community Land Model (CLM), NCAR Tech.
539 Note NCAR/TN-503+ STR, Boulder, Colo., 420pp, 2013.

540 Pellarin, T., Laurent, J. P., Cappelaere, B., Decharme, B., Descroix, L., and Ramier, D.: Hydrological
541 modelling and associated microwave emission of a semi-arid region in South-western Niger.
542 *Journal of Hydrology*, 375, 262–272, 2009.

543 Robock, A., Vinnikov, K. Y., Srinivasan, G., Entin, J. K., Hollinger, S. E., Speranskaya, N. A., Liu, S.
544 X., and Namkhai, A.: The Global Soil Moisture Data Bank, *Bull. Amer. Meteor. Soci.*, 81, 1281-
545 1299, 2000.

546 Robock, A., Mu, M., Vinnikov, K., Trofimova, I. V., and Adamenko T. I.: Forty-five years of observed
547 soil moisture in the Ukraine: No summer desiccation (yet), *Geophys. Res. Lett.*, 32, L03401,
548 doi:10.1029/2004GL021914, 2005.

549 Siebert, S., Döll, P., Hoogeveen, J. , Faures, J. M., Frenken, K., and Feick, S.: Development and
550 validation of the global map of irrigation areas, *Hydrology and Earth System Sciences*, 9, 535–547,
551 2005.

552 Sen, P. K.: Estimates of the regression coefficient based on Kendall’s tau, *J. Amer. Stat. Assoc.*, 63,
553 1379–1389, 1968.

554 Seneviratne, S., Corti, T., Davin, E., Hirschi, M., Jaeger, E., Lehner, I., Orlowsky, B., and Teuling, A.:
555 Investigating soil moisture–climate interactions in a changing climate: A review, *Earth-Sci. Rev.*,
556 99, 125–161, 2010.

557 Sheffield, J. , Goteti, G. , and Wood, E. F.: Development of a 50-year high-resolution global dataset of
558 meteorological forcings for land surface modeling, *J. Climate*, 19(13), 3088--3111, 2006.

559 Smith, A. B., Walker, J. P., Western, A. W., Young, R. I., Ellett, K. M., Pipunic, R. C., Grayson, R. B.,
560 Siriwardena, L., Chiew, F. H. B., and Richter, H.: The Murrumbidgee soil moisture monitoring
561 network dataset. *Water Resources Research*, 48(7), 7701, 2012.

562 Taylor, and Karl, E.: Summarizing multiple aspects of model performance in a single diagram, *Journal*
563 *of Geophysical Research*, 106(D7):7183, 2001.

564 Van Den Hurk, B., Best, M., Dirmeyer, P., Pitman, A., Polcher, J., and Santanello, J.: Acceleration of
565 Land Surface Model Development over a Decade of Glass, *Bull. Amer. Meteor. Soci.*, 92, 1593–
566 1600. doi:10.1175/BAMS-D-11-00007.1, 2011.

567 Van Den Hurk, B., Kim, H. J., Krinner, G., Seneviratne, S.I., Derksen, C., Oki, T., Douville, H., Colin,
568 J., Ducharne, A., Cheruy, F., Viovy, N., Puma, M.J., Wada, Y., Li, W., Jia, B. H., Alessandri, A.,
569 Lawrence, D.M., Weedon G.P., Ellis, R., Hagemann, S., Mao, J., Flanner, M.G., Zampieri, M.,
570 Materia, S., Law, R.M., Sheffield, J.: LS3MIP (V1.0) contribution to CMIP6: The Land Surface,
571 Snow and Soil moisture Model Intercomparison Project – aims, setup and expected outcome,
572 *Geosci. Model Dev.*, 9, 2809–2832, 2016.

573 Viovy, N., and Ciais, P.: A combined dataset for ecosystem modelling:
574 <http://esgf.extra.cea.fr/thredds/catalog/store/p529viov/cruncep/catalog.html>, last access: 1 August
575 2016, 2009.

576 Wada, Y., Van Beek, L. P. H., Wanders, N., and Bierkens, M. F. P.: Human water consumption
577 intensifies hydrological drought worldwide, *Environmental Research Letters*, 2013,
578 8(3):034036,2013.

579 Wagner, W., Lemoine, G., and Rott, H.: A method for estimating soil moisture from ERS scatterometer
580 and soil data, *Remote Sens. Environ.*, 70(2), 191-207, 1999.

581 Wang, A. H., and Zeng, X. B.: Sensitivities of terrestrial water cycle simulations to the variations of
582 precipitation and air temperature in China, *J. Geophys. Res: Atmospheres*, 2011, 116(D2) , 2011.

583 Weedon, G. P., Balsamo, G., Bellouin, N., Gomes, S., Best, M. J., and Viterbo, P.: The WFDEI
584 meteorological forcing dataset: WATCH Forcing Data methodology applied to ERAInterim
585 reanalysis data, *Water Resour. Res.*, 50, 7505–7514, 2014.

586 Wei, J., Dirmeyer, P. A., and Guo, Z.: Sensitivities of soil wetness simulation to uncertainties in
587 precipitation and radiation, *Geophys. Res. Lett.*, 35, L15703. doi:10.1029/2008GL034494, 2008.

588 Wentz, F. J., Ricciardulli, L., Hilburn, K. and Mears, C.: How Much More Rain Will Global Warming
589 Bring? *Science* 13, 233–235, 2007.

590 Wissler, D., Fekete, B. M., Vörösmarty, C. J. and Schumann, A. H.: Reconstructing 20th century global
591 hydrography: a contribution to the global terrestrial network-hydrology (GTNH), *Hydrol. Earth
592 Syst. Sci.*, 14 1–24, 2010

593 Xie Z. H., Liu S., Zeng Y. Y., Gao J. Q., Qin P. H., Jia, B. H., Xie, J. B., Liu, B., Li, R. C., Wang, Y.,
594 and Wang, L. H.: A high-resolution land model with groundwater lateral flow, water use and soil
595 freeze-thaw front dynamics and its applications in an endorheic basin, *J. Geophys. Res.-Atmos.*,
596 123, 7204-7222. <https://doi.org/10.1029/2018JD028369>, 2018.

597 Yin, Z., Ottlé, C., Ciais, P., Guimberteau, M., Wang, X. H., Zhu, D., Maignan, F., Peng, S. S., Piao, S.
598 L., Polcher, J., Zhou, F., Kim, H., and other China-Trend-Stream project members.: Evaluation of
599 ORCHIDEE-MICT-simulated soil moisture over China and impacts of different atmospheric

600 forcing data, *Hydrol. Earth Syst. Sci.*, 22, 5463–5484, <https://doi.org/10.5194/hess-22-5463-2018>,
601 2018.

602 Yu, Y., Xie, Z. H., and Zeng, X. B.: Impacts of modified Richards equation on RegCM4 regional climate
603 modeling over East Asia, *J. Geophys. Res.-Atmos.*, 119, 12642–12659, doi:10.1002/2014jd021872,
604 2014.

605 Zeng, Y. Y., Xie, Z. H., and Liu, S.: Seasonal effects of irrigation on land-atmosphere latent heat,
606 sensible heat, and carbon fluxes in semiarid basin, *Earth System Dynamics*, 8(1), 113–127, 2017.

607 Zeng, Y. Y., Xie, Z. H., Yu, Y., Liu, S., Wang, L. Y., Zou, J., Qin, P. H., and Jia, B. H.: Effects of
608 anthropogenic water regulation and groundwater lateral flow on land processes, *Journal of*
609 *Advances in Modeling Earth Systems*, 8(3), 1106–1131, 2016a.

610 Zeng, Y. Y., Xie, Z. H., and Zou, J.: Hydrologic and climatic responses to global anthropogenic
611 groundwater extraction, *J. Climate*, 30. 10.1175/JCLI-D-16-0209.1, 2016b.

612 Zhan, X., Zheng, W., Fang, L., Liu, J., Hain, C., Yin, J., and Ek, M.: A preliminary assessment of the
613 impact of SMAP soil moisture on numerical weather forecasts from GFS and NUWRF models,
614 IGARSS 2016 - 2016 IEEE International Geoscience and Remote Sensing Symposium, IEEE,
615 5229–5232, 2016.

616 Zou, J., Xie, Z. H., Yu, Y., Zhan, C. S., and Sun, Q.: Climatic responses to anthropogenic groundwater
617 exploitation: A case study of the Haihe River Basin, northern China, *Climate Dyn.*, 42, 2125–2145,
618 2014.

619

Tables

620

Table 1. General information of the meteorological forcing datasets

Data	Spatial	Interval	Time period	Source
GSWP	0.5°	3-hourly	1901–2012	[Kim et al., 2016]
WFD/WFDEI	0.5°	3-hourly	1901–2000/1979–2014	[Haddeland et al., 2011; Weedon et al., 2014]
CRU-NCEP	0.5°	6-hourly	1901–2010	[Viovy and Ciais, 2009]
PRINCETON	0.5°	3-hourly	1901–2012	[Sheffield et al., 2006]

621

622

Table 2. Details for the stations used in this study.

Continent	Network name	Country	Number of sites used	Depths (m)	Corresponding simulated soil layer	References
Africa	AMMA-CATCH	Benin, Niger	4	0.05;0.2,0.4	3,5,6	Cappelaere et al. (2009); de Rosnay et al. (2009); Mougin et al. (2009); Pellarin et al. (2009)
Australia	OZNET	Australia	8	0–0.3;0.3–0.6; 0.6–0.9	1–5;6–7;7	Smith et al. (2012)
Europe	SMOSMANIA, ORACLE, SWEX_POLAND	France, Poland	20	0.05;0.1; 0.2;0.3	3;4;5;6	Albergel et al. (2008); Calvet et al. (2008); https://bdoh.irstea.fr/ORACLE/ Marczewski et al. (2010) http://www.wcc.nrcs.usda.gov/snow/
North America	SNOTEL, SCAN	US	82	0.05;0.2;0.5	3;5;6–7	http://www.wcc.nrcs.usda.gov/scan/
Asia	IIT_KANPUR	India	1	0.1;0.25; 0.5;0.8	4;5;6–7;7	http://www.iitk.ac.in/
Asia	CHINA	China	40	0–0.1;0.1–0.2; 0.2–0.3;0.3–0.5	1–3;4;5;7	Robock et al. (2000)

Asia	MONGOLIA	Mongolia	28	0-0.1,0.1-0.2, 0.2-0.3	1-3;4;5	Robock et al. (2000)
Asia	RUSWET- GRASS	Former Soviet Union	30	0-0.1,0-1	1-3;1-8	Robock et al.(2000)

624

625

626 **Table 3.** Trends in NEW simulated surface soil moisture and precipitation and
 627 temperature of forcing data. * = $p < 0.05$.

NEW	SM ($\text{m}^3\text{m}^{-3}\text{yr}^{-1}$)	Pre (mmyr^{-1})	Tem ($^{\circ}\text{C yr}^{-1}$)
GSWP	* $-0.89\text{e-}4$	-0.16	*0.017
CRU-NCEP	* $-0.97\text{e-}4$	-0.27	*0.017
PRINCETON	$-0.65\text{e-}4$	-0.008	*0.017
WFD	* $-0.15\text{e-}3$	*-1.96	*0.019

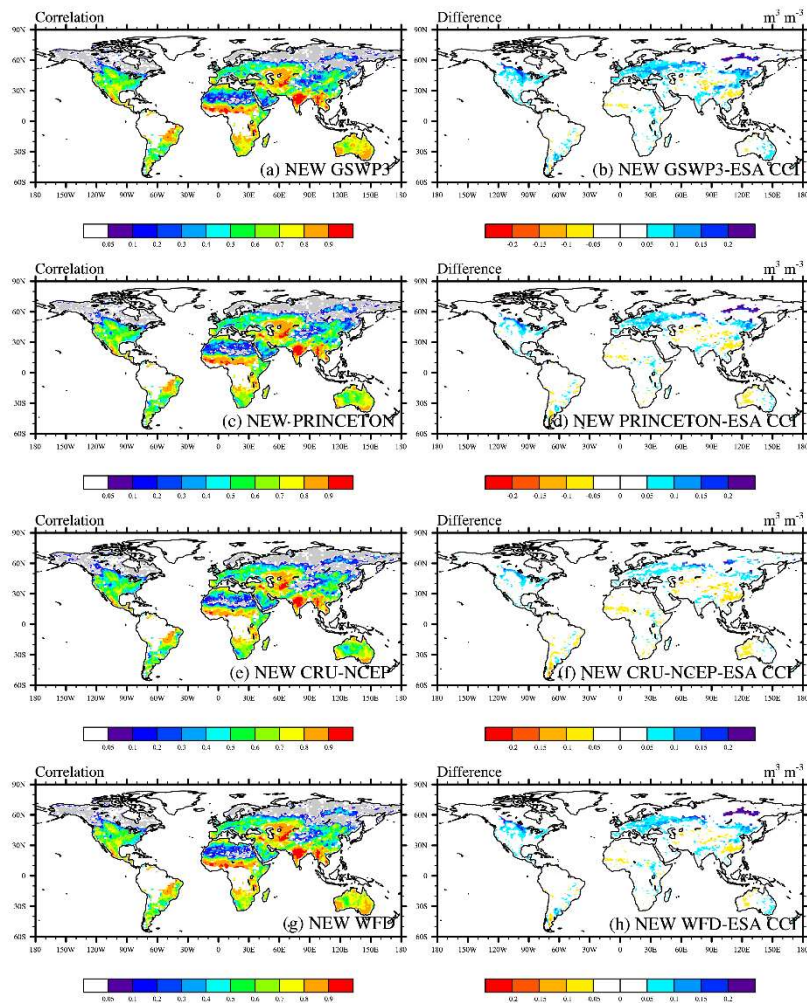
628

629

630

Figures

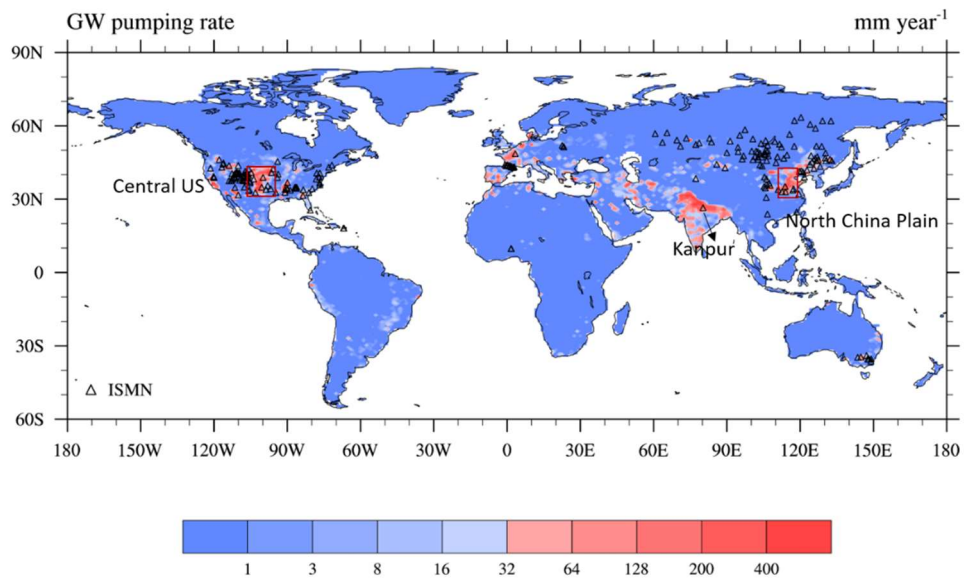
631



632

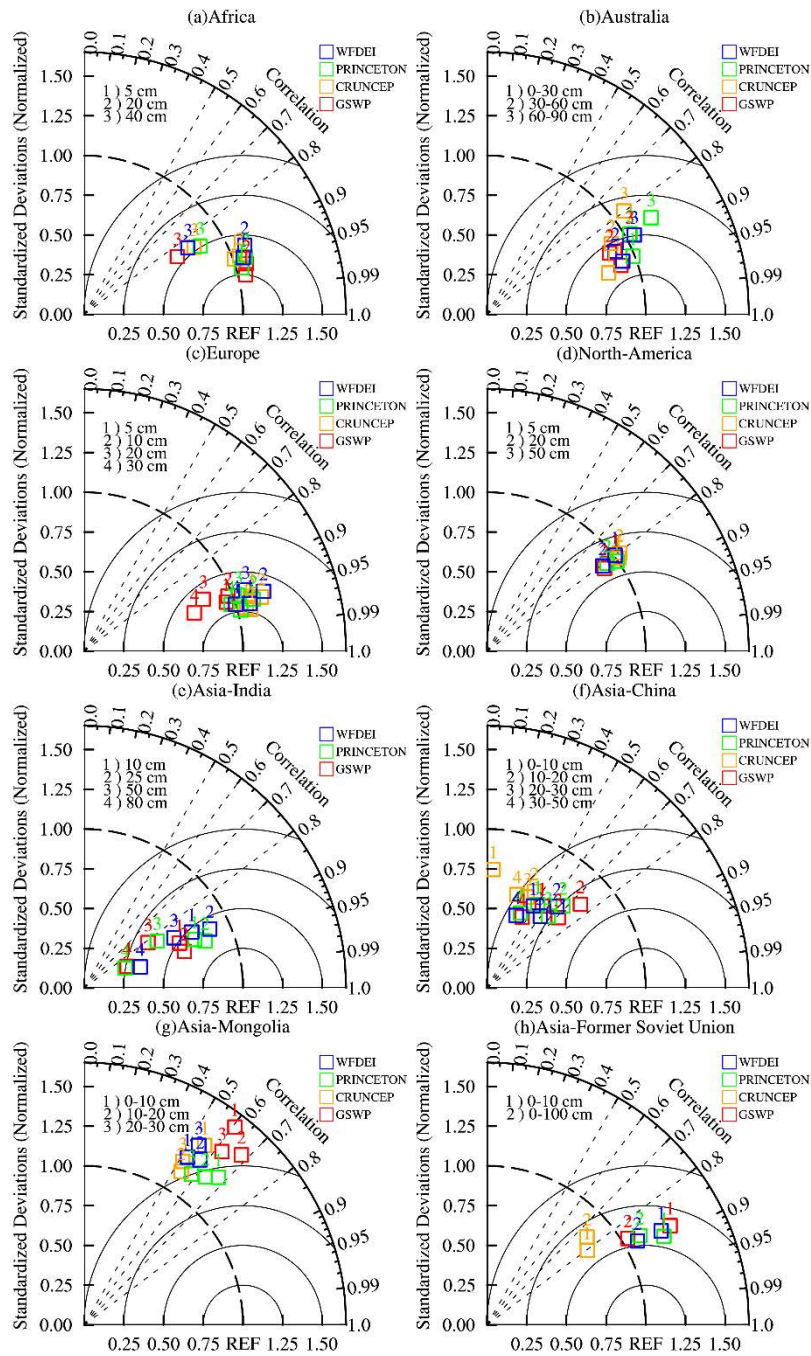
633 **Figure 1.** Correlation coefficients (a, c, e, g) and differences of spatial patterns (b, d, f, h) of the ESA CCI soil
634 moisture and the corresponding simulated top 10 cm soil moisture from 1979–2010. Gray pixels indicate no
635 correlation and negative correlation.

636



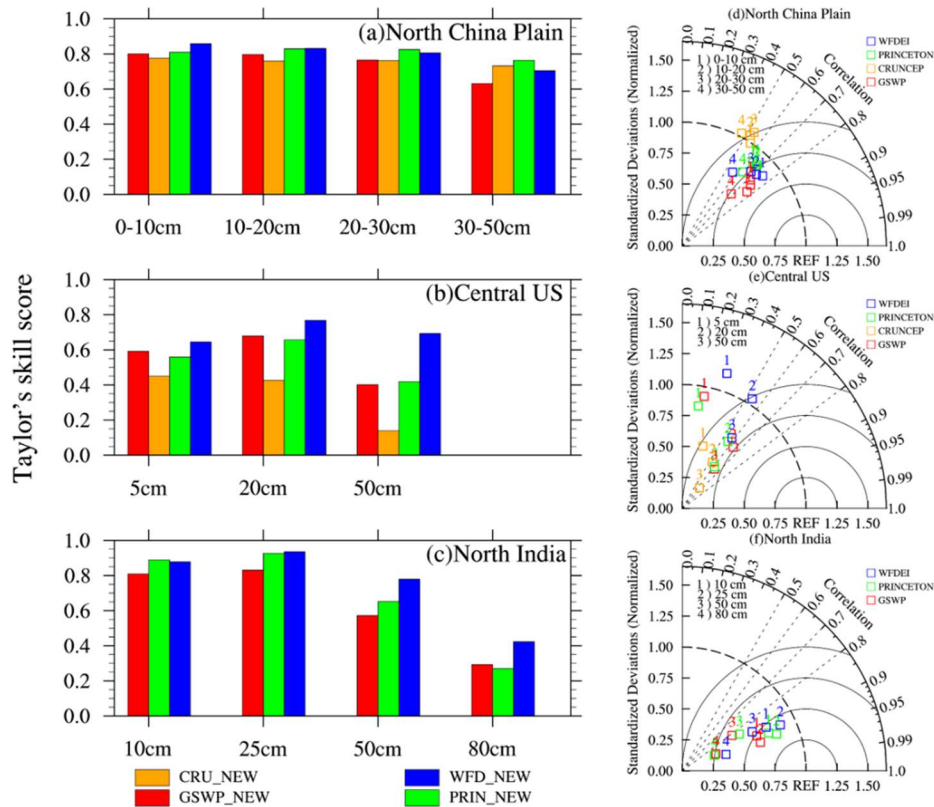
637
 638
 639
 640

Figure 2. Distribution of soil moisture stations and three subregions. Seven stations on the North China Plain, 15 in central US, and one in Kanpur of North India). The background is the groundwater (GW) extraction rate.



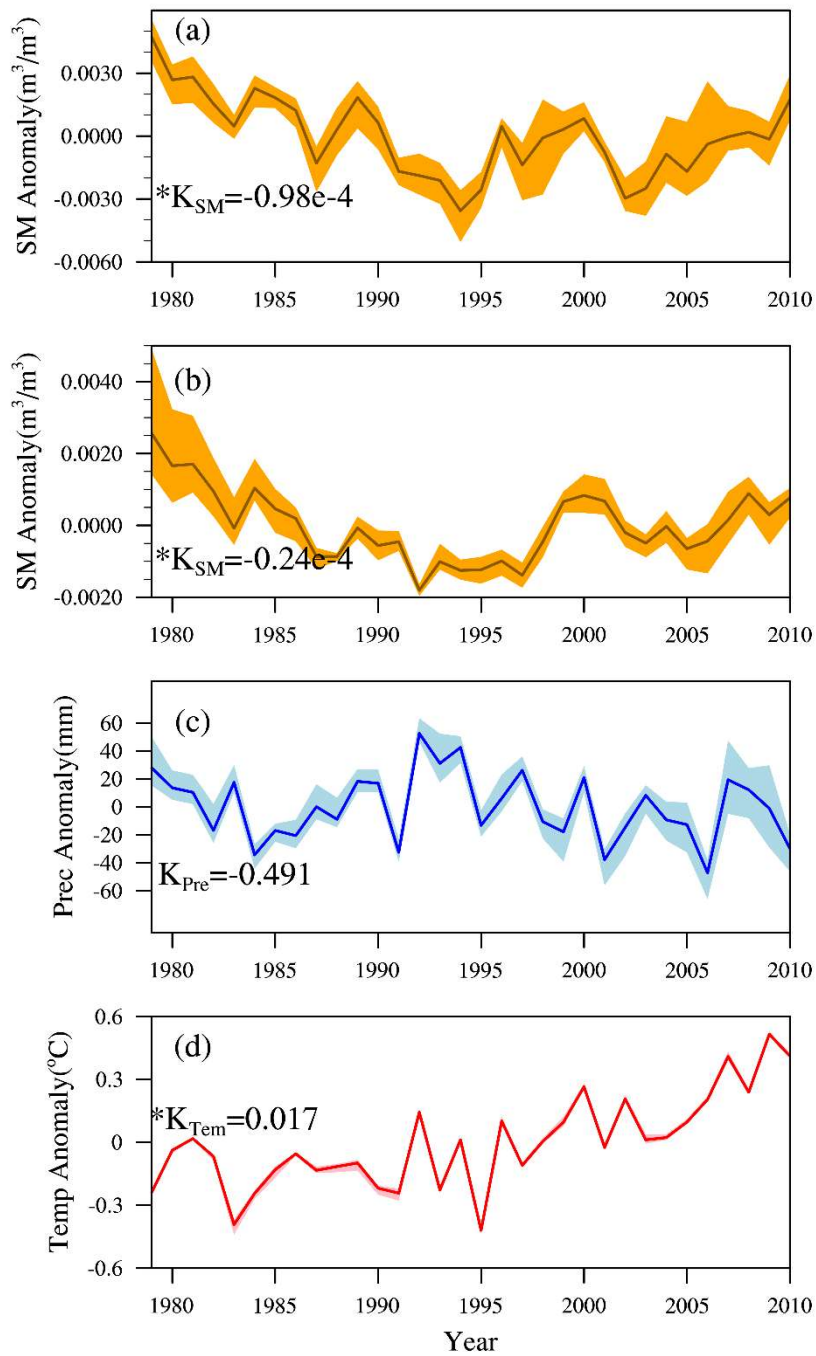
641

642 **Figure 3.** Taylor diagrams illustrating the comparisons among GSWP, CRUNCEP, PRINCETON, WFDEI, and in-
 643 situ observation data.



644

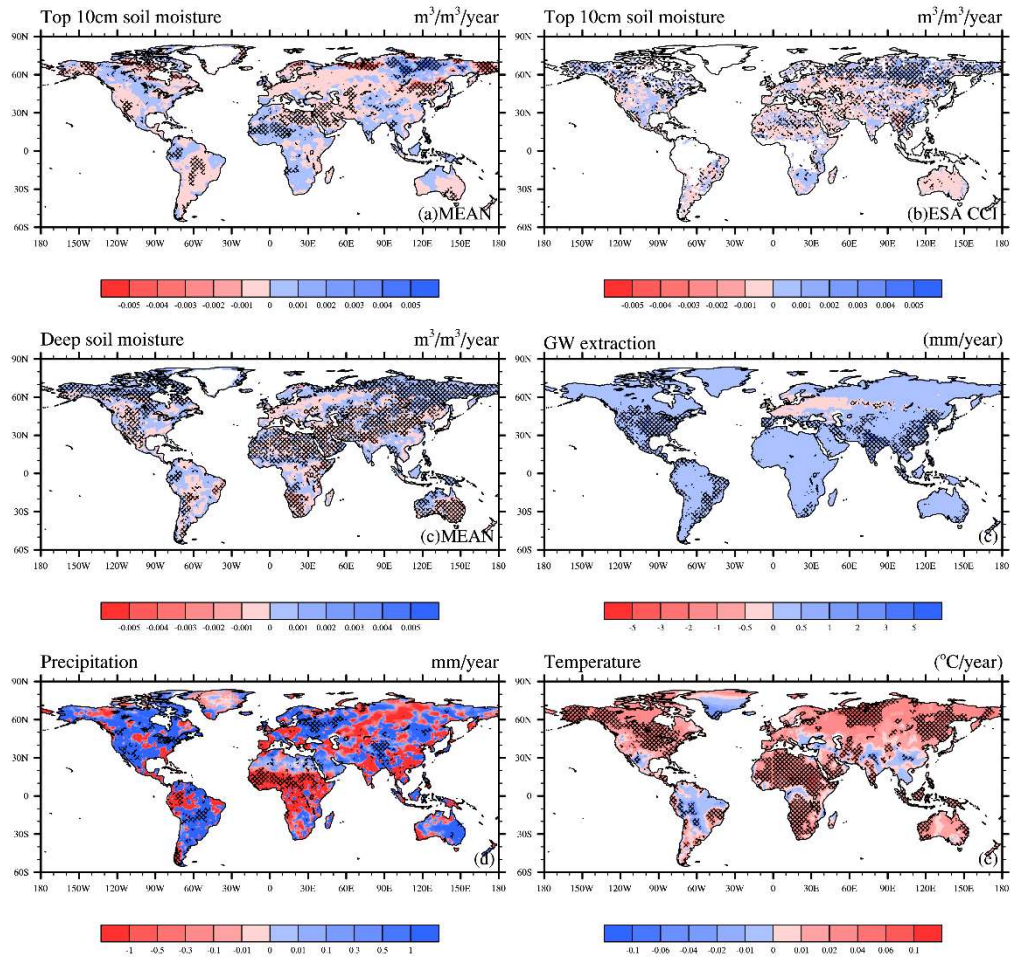
645 **Figure 4.** Taylor's skill scores and Taylor diagrams illustrating the comparisons among GSWP, CRUNCEP,
 646 PRINCETON, WFDEI, and in-situ observations. (a, d) North China Plain; (b, e) Colorado of Central US;
 647 North India. The azimuthal angle represents the correlation coefficient, and radial distance is the standard deviation
 648 normalized to observations.



649

650 **Figure 5.** Annual mean of (a) surface soil moisture, (b) deep soil moisture, (c) precipitation, and (d) temperature
 651 averaged globally from 1979–2010. * = $p < 0.05$.

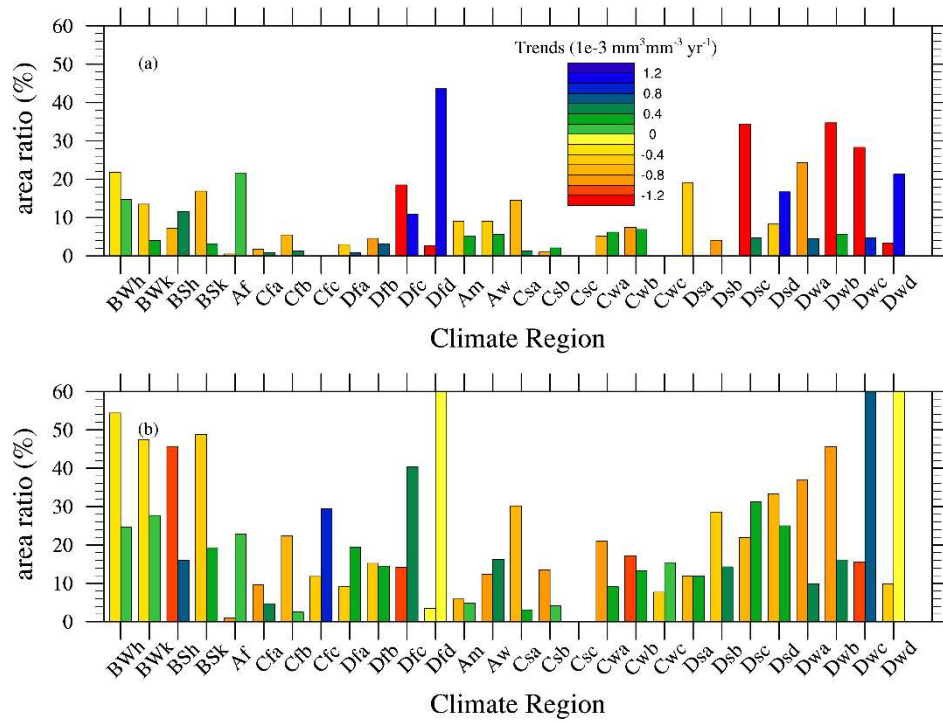
652



653

654 **Figure 6.** The spatial distribution of linear trends for (a) and (b) surface soil moisture ($\text{m}^{-3} \text{yr}^{-1}$), (c) deep soil
 655 moisture ($\text{m}^{-3} \text{yr}^{-1}$), (d) and (e) precipitation (mm yr^{-1}), temperature ($^{\circ}\text{C yr}^{-1}$), groundwater extraction (mm yr^{-1}).
 656 The shaded areas represent grids with statistically significant trends ($p < 0.05$).

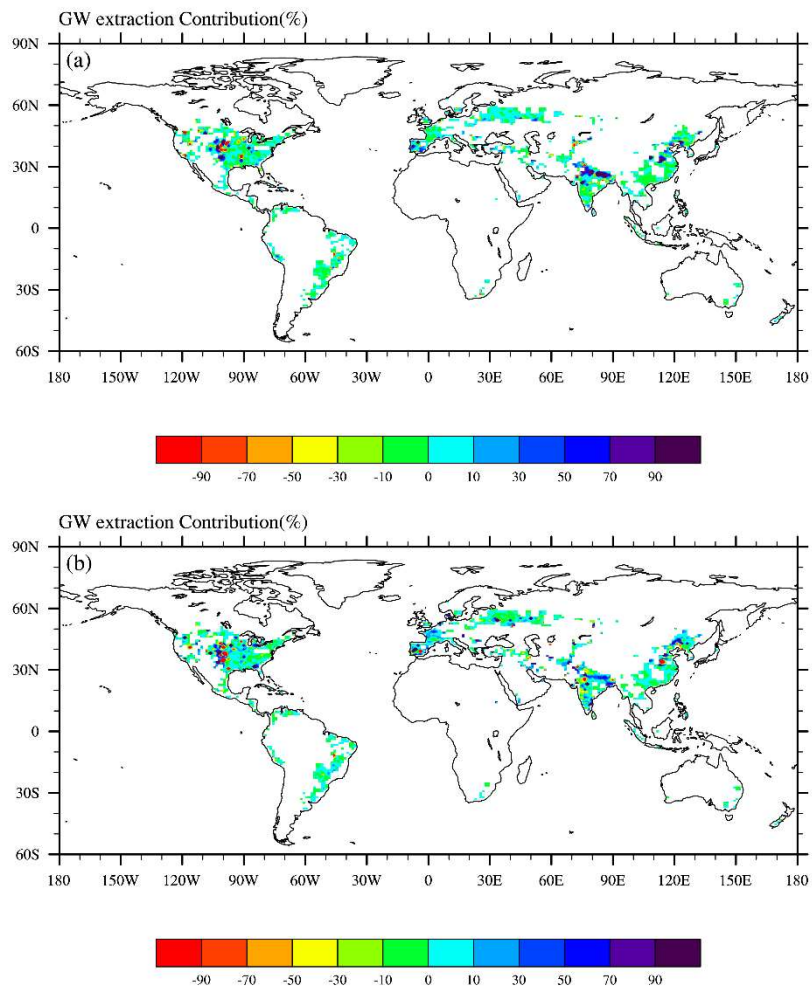
657



658

659 **Figure 7.** Statistics of the soil moisture trends. (a, b) The ratio of surface and deep soil moisture to wet and dry for
 660 28 Köppen-Geiger climate types. For each type, the left bar is the drying ratio and the right bar is the wetting ratio.

661

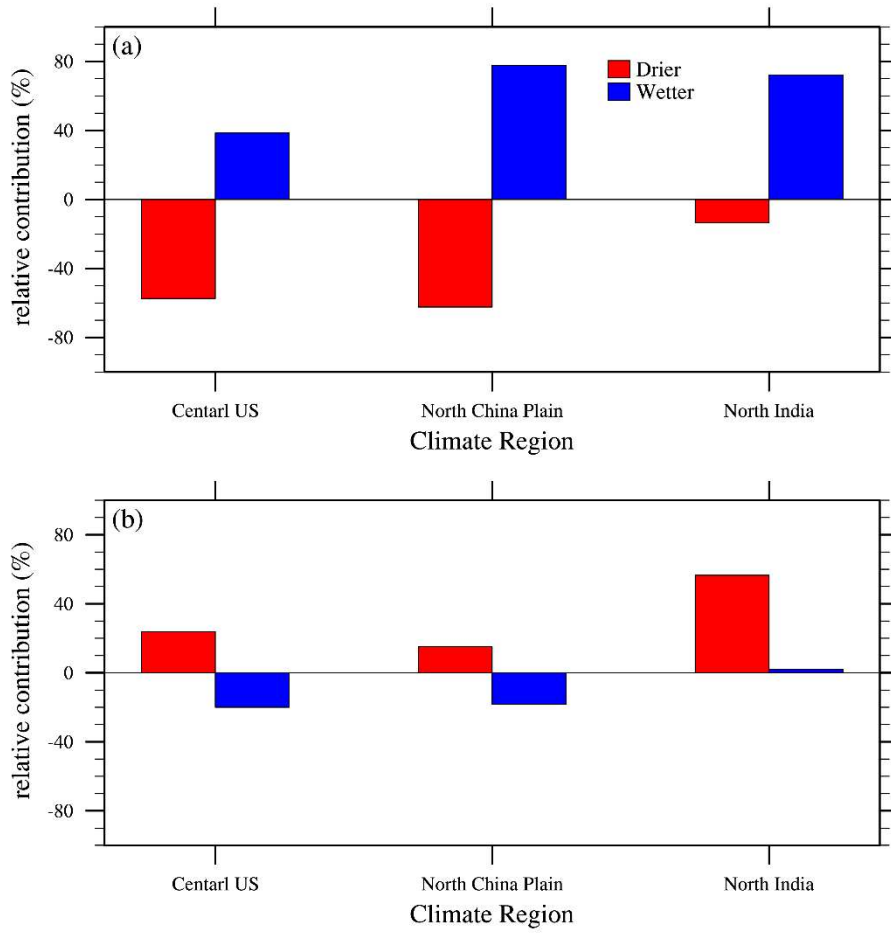


663

664

665 **Figure 8.** The relative contribution of groundwater extraction to (a) surface and (b) deep soil moisture trends (%).

666



667

668 **Figure 9.** The relative contribution of GW extraction to regional (a) surface, (b) deep soil moisture trends (%). North
 669 China Plain (34N–40N, 110E–120E), northern India (23N–33N, 68E–78E), central US (33N–42N, 97W–105W).